^{1}H NMR Investigation of the Electronic Structure of the Four-Iron Ferredoxin from the Hyperthermophilic Archaeon *Thermococcus litoralis*

Antonio Donaire,†,‡ Carol M. Gorst,† Z. H. Zhou,§ Michael W. W. Adams,§ and Gerd N. La Mar*,†

Contribution from the Department of Chemistry, University of California, Davis, California 95616, and Department of Biochemistry, University of Georgia, Athens, Georgia 30602

Received March 2, 1994•

Abstract: The oxidized and reduced forms of the four-iron ferredoxin from the hyperthermophilic archaeon, *Thermococcus litoralis* (*Tl*), have been investigated by ^{1}H NMR spectroscopy. All three protons for each of the four Cys are located by 2D and 1D NMR experiments, although differentiation of α- and β-protons required the interpretation of steady-state NOEs and relaxation properties of the signals. The complete correlation between the Cys signals in the reduced and oxidized ferredoxin was carried out by 2D EXSY and steady-state saturation-transfer NMR, and an electron self-exchange rate of $\sim 5 \times 10^4$ M^{-1} s^{-1} at 30 °C, pH 7.6, is estimated. The β-protons for two ligated Cys exhibit Curie-like temperature dependence, and the other two display anti-Curie temperature dependence, indicative of the iron atoms arising from the mixed-valence pair with intermediate $S = {}^9/_2$, and the diferrous pair with intermediate $S = 4$, respectively. Standard 2D identification of the protons for nonligated residues which have significant dipolar contacts with the ligated Cys provide the sequence-specific assignment for Cys 18 and Cys 16. The two remaining ligated Cys are shown to be sequence-specifically assignable upon qualitative consideration of the relative relaxation properties of the ligated Cys α-protons, as predicted by the pattern of Cys orientations relative to the cluster in numerous crystallographically characterized bacterial ferredoxins. The combined assignments identify Cys 10 and Cys 16 as ligated to the valence-delocalized iron atoms in the reduced ferredoxin. Comparison of the NMR spectra of the reduced four-iron and oxidized three-iron *Tl* ferredoxins indicates a similar pairing of the iron atoms in the spin coupling hierarchy. The patterns of both relaxation properties and contact shifts of α-protons for ligated Cys are discussed in terms of the geometry of the ligand.

Introduction

Ferredoxins, Fd,[1] are small electron-transfer proteins containing an iron–sulfur cluster.[2-6] The two major classes are the 2Fe plant-type Fd, with cluster oxidation states designated by $[Fe_2S_2]^{+,2+}$, and the bacterial or cubane Fd, which occur primarily in the 4Fe (or 2 × 4Fe) form with $[Fe_4S_4]^{+,2+}$ but also exist as a 3Fe (or 3Fe + 4Fe) form with $[Fe_3S_4]^{0,+}$. These proteins exhibit a remarkably wide range of redox potentials for the cluster as a whole, despite highly analogous active site architectures. Additionally, a clear distinction exists between the redox potentials of individual iron atoms or pairs of iron atoms within a cluster, as revealed by Mössbauer spectroscopy.[6,7] For example, the reduced $[Fe_2S_2]^+$ cluster possesses distinct Fe^{3+} and Fe^{2+}, and oxidized $[Fe_4S_4]^{2+}$ cluster has four $Fe^{2.5+}$, while the reduced $[Fe_4S_4]^+$ cluster has two $Fe^{2.5+}$ and two $Fe^{2.0+}$. Another 4Fe bacterial protein, the high-potential iron–sulfur protein,[2] HiPiP, $[Fe_4S_4]^{2+,3+}$, is analogous to oxidized Fd in its reduced form and in its oxidized form contains $2Fe^{3.0+}$ and $2Fe^{2.5+}$. Hence, in the 2Fe Fd, the transferred electron is localized, while in all 4Fe clusters, this electron is valence-delocalized over a pair of iron atoms.[2,3,5,6] The tendency for 2Fe systems to exhibit localized valence while 4Fe clusters exhibit delocalized valence over pairs of iron appears to be an intrinsic quantum mechanical property of the cluster and does not relate to protein perturbations.[8,9] Identification of the ferric ion that is reduced in 2Fe Fd or the pair of $Fe^{2.5+}$ in oxidized 4Fe Fd that is reduced may reveal protein influences designed to control the flow of electrons. The oxidation states of individual or pairs of iron atoms and the structural constraints that modulate both the local and cluster redox potentials are subjects of considerable interest.[10]

The nature of the effective valence state of individual iron atoms in even-iron clusters with an odd number of electrons[11-16] and their location in the protein topology[17-23] are most effectively

* Author to whom correspondence should be addressed.
† University of California.
§ University of Georgia.
‡ Permanent address: Departament de Química Inorgánica, Faculat de Química, Universitat de Valéncia, Doctor Moliner, 50, 46100 Burjassot, Valéncia, Spain.

• Abstract published in *Advance ACS Abstracts*, July 1, 1994.

(1) Abbreviations used: Fd, ferredoxin; HiPiP, high-potential iron–sulfur protein; *Tl*, *Thermococcus litoralis*; *Dq*, *Desulfovibrio gigas*; *Pa*, *Peptococcus aerogenes*; *Bt*, *Bacillus thermoproteolyticus*; *Av*, *Azotobacter vinlandiui*; *Pf*, *Pyrococcus furiosus*; *Cp*, *Clostridium pasteurianum*; *Cau*, *Clostridium acidi urici*.

(2) Cammack, R.; Dickson, D.; Johnson, C. In *Iron Sulfur Proteins*; Lovenberg, W., Ed.; Academic Press: New York, 1977; Vol. III, pp 283–330.
(3) Thompson, A. J. In *Metalloproteins*; Hanson, P., Ed.; Verlag Chemie: Weinheim, FRG, 1985; Part I, pp 79–120.
(4) Beinert, H. *FASEB J.* **1990**, *4*, 2483–2494.
(5) Howard, J. B.; Rees, D. C. *Adv. Protein Chem.* **1991**, *42*, 199–281.
(6) Cammack, R. In *Advances in Inorganic Chemistry*; Cammack, R., Ed.; Academic Press: San Diego, CA, 1992; Vol. 38, pp 281–322.
(7) Münck, E.; Papaefthymiou, V.; Surerus, K. K.; Girerd, J.-J. In *Metal Clusters in Proteins*; Que, L., Ed.; ACS Symposium Series 372; American Chemical Society: Washington, DC, 1988; p 302–325.
(8) Holm, R. H.; Ibers, J. A. In *Iron Sulfur Proteins*; Lovenberg, W., Ed.; Academic Press: New York, 1977; Vol. III, pp 206–281.
(9) Noodleman, L.; Case, D. A. In *Advances in Inorganic Chemistry*; Cammack, R., Ed.; Academic Press: San Diego, CA, 1992; Vol. 38, pp 423–470.
(10) Langen, R.; Jensen, G.; Jacob, U.; Stephens, J.; Warshel, A. *J. Biol. Chem.* **1992**, *267*, 25625–25627.
(11) Phillips, W. D.; Poe, M. In *Iron Sulfur Proteins*; Lovenberg, W., Ed.; Academic Press: New York, 1973; Vol. II, pp 255–285.
(12) Dunham, W. R.; Palmer, G.; Sands, R. H.; Bearden, R. J. *Biochim. Biophys. Acta* **1971**, *253*, 373–384.
(13) Banci, L.; Bertini, I.; Luchinat, C. *Struct. Bonding* **1990**, *72*, 113–135.
(14) Luchinat, C.; Ciurli, S. In *Biological Magnetic Resonance*; Berliner, L. J., Reuben, J., Eds.; Plenum Press: New York, 1993; pp 357–420.
(15) Bertini, I.; Briganti, F.; Luchinat, C.; Scozzafava, A.; Sola, M. *J. Am. Chem. Soc.* **1991**, *113*, 1237–1245.
(16) Bertini, I.; Briganti, F.; Luchinat, C.; Messori, L.; Mannanni, R.; Scozzafava, A.; Vallini, G. *Eur. J. Biochem.* **1992**, *204*, 831–835.

0002-7863/94/1516-6841$04.50/0

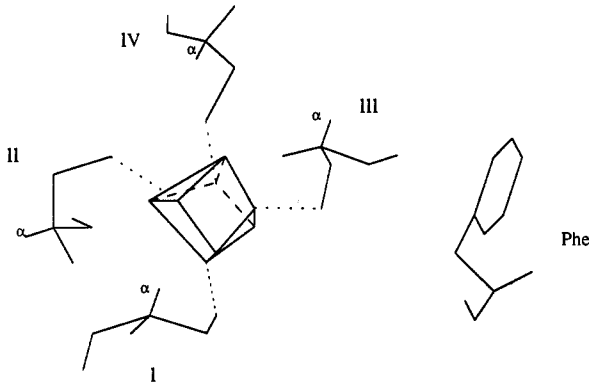

Figure 1. Schematic representation of the coordination of the four conserved cysteines (labeled I–IV in the order they appear in the sequence Cys 10, 13, 16, 51 in *Tl* Fd) in 4Fe ferredoxin clusters. Cys II is either replaced or not coordinated in 3Fe ferredoxin. The position of the highly conserved Phe (Phe 24 in *Tl* Fd) near Cys III (Cys 16 in *Tl*) is shown.

addressed by NMR spectroscopy. These necessarily paramagnetic states result in unique spin magnetization $\langle S_z \rangle_i$ at each iron which is sensed by the ^{1}H contact shift of the cysteine coordinated to that iron.[12-14] The location and sequence-specific assignment of each Cys in reduced 2Fe Fd,[17,18] oxidized HiPiP,[19-21] and reduced 2 × 4Fe Fd[23] have identified the individual valence states of all of the iron atoms. NMR discrimination of the valence states is based on the spin coupling that accounts for the magnetic properties of cubane clusters[6,7,12-14] (*i.e.*, structure as in Figure 1). Pairs of valence-delocalized high-spin iron atom spins couple ferromagnetically (*i.e.*, in reduced 4Fe Fd, $2Fe^{2.0+}$ for Fe_1,Fe_2 yield $\vec{S}_1 + \vec{S}_2 = S_A = 4$, and $2Fe^{2.5+}$ for Fe_3,Fe_4 yield $\vec{S}_3 + \vec{S}_4 = S_B = {}^9/_2$), with the intermediate spins, S_A and S_B, coupling antiferromagnetically to yield a total cluster spin $S_T = S_A + S_B = {}^1/_2$. Both S_A and S_B align with the applied field (low-field contact shift) at high temperature. At low temperature, however, the larger of the two intermediate spins, S_B, aligns parallel with the field (low-field contact shifts), and the smaller intermediate spin, S_A, necessarily aligns antiparallel to the field (upfield contact shifts).[12-14] The net result is that the valence-delocalized pair of iron atoms, $2Fe^{2.5+}$ with $S_B = {}^9/_2$, is predicted to exhibit Curie-like temperature dependence, while the pair of $Fe^{2.0+}$ with $S_A = 4$ will exhibit anti-Curie temperature dependence for the ligated Cys contact shift.[15,16]

To date there is no reduced single cluster 4Fe Fd for which the Cys ligating to the valence-delocalized iron atoms has been identified sequence-specifically. Such assignments, however, have been recently reported[23] for the reduced 2 × 4Fe Fd from *Clostridium acidic urici* (*Cau*) and *Clostridium pasteurianum* (*Cp*). The NMR studies designed to uniquely identify the sequence basis for differentiation of the valence-delocalized pairs have been carried out primarily on oxidized HiPiP.[15,19-21] The assignments of coordinated Cys signals in HiPiP are greatly facilitated by their proximity to several different aromatic side chains,[2,24] which resonate in a unique spectral window and exhibit relatively large shift dispersion. Fds, in contrast, generally possess fewer aromatic residues. In the single but not the double cluster 4Fe Fd, an aromatic residue is conserved[25] in the hydrophobic core near the cluster (Figure 1). On the other hand, some Fd can exist in both a 3Fe and a 4Fe form.[7,22,26-28] Careful comparison of the Cys hyperfine shift patterns in the 3Fe and 4Fe forms will be shown to provide valuable information for making the necessary assignments. The oxidized 3Fe Fd, moreover, exhibits a 2:1 asymmetry in the valence-state and/or spin coupling pattern[7,29,30] and therefore provides an interesting example for examining the structural basis for the asymmetry among the iron in two different cluster architectures.

In this report we address the ^{1}H NMR spectral properties of the cluster-ligated Cys in both oxidation states of the 4Fe Fd from the hyperthermophilic archaeon *Thermococcus litoralis* (*Tl*), a 59-residue protein that can exist in both 3Fe and 4Fe forms.[28] This organism thrives near 100 °C in sulfide-rich marine environments, and the purified protein can be incubated at 90 °C for 24 h without detectable degradation.[31] The protein represents an interesting candidate for elucidating the sequence control of the delocalized valence pair, as well as for solution ^{1}H NMR structure determination to provide insight into the basis for its remarkable thermostability. Identification of three sets of Cys C_βH signals in oxidized 3Fe *Tl* Fd has been reported, but only one Cys could be sequence-specifically assigned.[29] The sequence[28] of *Tl* Fd is given in Figure 2, where it is compared with that of *Desulfovibrio gigas*[32] (*Dg*) Fd, whose 3Fe form has yielded a high-resolution crystal structure.[33] The alignment is made on the basis of the six conserved Cys, of which those labeled I–IV provide the ligating residues for the cluster, while Cys V and VI may participate in a disulfide bridge. The disulfide bridge is formed in oxidized *Dg* 3Fe Fd.[33] *Tl* and *Dg* Fd exhibit significant sequence homology,[28,32] particularly for the 23 residues after Cys I, of which the latter half form a hydrophobic core that includes the conserved aromatic residue[25,32] in single 4Fe cluster Fd.

Experimental Section

Proteins. *T. litoralis* cultures were grown and the purification of its ferredoxin was carried out as previously described.[34] The samples for NMR spectroscopy were equilibrated with sodium phosphate buffer, 50 mM, pH 7.6 and exchanged into 100% ^2H_2O in an Amicon ultrafiltration device. Reduced samples were prepared in an anaerobic glove box and contained 2 mM dithionite. The final concentration of the samples ranged between 5 and 9 mM.

NMR Spectroscopy. The ^{1}H NMR spectra were recorded at 500 MHz on a General Electric Ω500 spectrometer and at 400 MHz on a Bruker AMX-400 spectrometer. Chemical shift values were referenced to 2,2-dimethyl-2-silapentane-5-sulfonate (DSS) through the residual solvent signal. 500-MHz ^{1}H NMR spectra were collected by the normal one pulse with ^1H_2O presaturation or the super-WEFT[35] pulse sequence over a range of repetition rates (0.4–10 s^{-1}) and delay times (50–225 ms)

(17) Dugad, L. B.; La Mar, G. N.; Banci, L.; Bertini, I. *Biochemistry* **1990**, *29*, 2263–2271.
(18) Skjeldal, L.; Westler, W. M.; Oh, B.-H.; Krazel, A. M.; Holden, H. M.; Jacobsen, B. L.; Rayment, I.; Markely, J. L. *Biochemistry* **1991**, *30*, 7363–7368.
(19) Nettesheim, D. G.; Harder, S. R.; Feinberg, B. A.; Otvos, J. D. *Biochemistry* **1992**, *31*, 1234–1244.
(20) Bertini, I.; Capozzi, F.; Ciurli, S.; Luchinat, C.; Messori, L.; Piccioli, M. *J. Am. Chem. Soc.* **1992**, *114*, 3332–3340.
(21) Banci, L.; Bertini, I.; Capozzi, F.; Carloni, P.; Ciurli, S.; Luchinat, C.; Piccioli, M. *J. Am. Chem. Soc.* **1993**, *115*, 3431–3440.
(22) Macedo, A. L.; Palma, P. N.; Moura, I.; LeGall, J.; Wray, V.; Moura, J. G. *Magn. Reson. Chem.*. **1993**, *31*, S59–S67.
(23) Bertini, I.; Capozzi, F.; Luchinat, C.; Piccioli, M.; Vila, A. *J. Am. Chem. Soc.* **1994**, *116*, 651–660.
(24) Markley, J. L.; Chan, T. M.; Krishnamoorthi, R.; Ulrich, E. In *Iron Sulfur Protein Research* Matsubara, H., Katsube, Y., Wada, K., Eds.; Japanese Science Society Press: Tokyo, 1986; pp 167–184.
(25) Otaka, E.; Ooi, T. *J. Mol. Evol.* **1987**, *26*, 257–267. Matsubara, H.; Saeki, K. In *Advances in Inorganic Chemistry*; Cammack, R., Ed.; Academic Press: San Diego, CA, 1992; Vol. 38, pp 223–280.
(26) Bruschi, M.; Hatchikian, E. C.; LeGall, J.; Moura, J. J. G.; Xavier, A. V. *Biochim. Biophys. Acta* **1976**, *449*, 225–285.
(27) Conover, R. C.; Park, J.-B.; Adams, M. W. W.; Johnson, M. K. *J. Am. Chem. Soc.* **1990**, *112*, 4562–4564.
(28) Zhou, Z. H.; Blamey, J. M.; Park, J.-B.; Magnuson, J. K.; Howard, J. B.; Hankins, H.; Johnson, M. K.; Adams, M. W. W., submitted for publication.
(29) Busse, S. C.; La Mar, G. N.; Yu, L. P.; Howard, J. B.; Smith, E. T.; Zhou, Z. H.; Adams, M. W. W. *Biochemistry* **1992**, *31*, 11952–11962.
(30) Macedo, A. L.; Moura, I.; Moura, J.; LeGall, J.; Huynh, B. H. *Inorg. Chem.* **1993**, *32*, 1101–1105.
(31) Neuner, A.; Jannasch, H. W.; Belkin, S.; Stetter, K. O. *Arch. Microbiol.* **1990**, *153*, 205–207.
(32) Travis, J.; Newman, O. J.; LeGall, J.; Peck, H. D. *Biochim. Biophys. Res. Commun.* **1971**, *45*, 452–458.
(33) Kissinger, C. R.; Sieker, L. C.; Adman, E. T.; Jensen, L. H. *J. Mol. Biol.* **1991**, *219*, 693–715.
(34) Mukund, S.; Adams, M. W. W. *J. Biol. Chem.* **1993**, *268*, 13592–13600.
(35) Inubushi, T.; Becker, E. D. *J. Magn. Reson.* **1983**, *51*, 128–133.

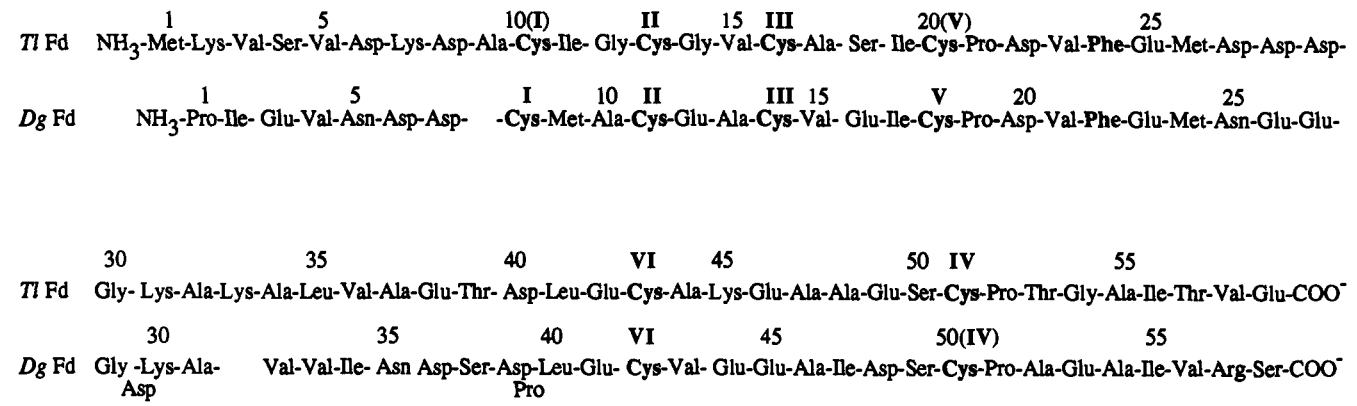

Figure 2, Amino acid sequence of the Fd for *T. litoralis* ferredoxin,[28] compared to that of *D. gigas* ferredoxin.[32] The alignment is based on conserved positions for the four cluster-ligating Cys **I–IV** and the two cysteines, **V** and **VI**, involved in a disulfide bridge[33] in *Dg* Fd.

in order to variably suppress the slowly relaxing diamagnetic envelope and enhance the broad, strongly relaxed Cys signals. The spectral width for oxidized Fd and reduced Fd were 20.0 and 52.6 kHz, respectively. Nonselective T_1 values were determined from the initial slope of the magnetization recovery in a standard inversion–recovery experiment. Line widths for resolved peaks were determined by fitting the entire hyperfine region to a series of Lorentzian lines. For unresolved peaks of interest, the line width was estimated from the line shape of the NOE response in a 1D NOE difference trace. Steady-state 1D NOE and saturation-transfer measurements were made using a super-WEFT pulse sequence. The selected resonance was irradiated for 95% of the relaxation delay time. Data were acquired by interleaving a block of scans with saturation on-resonance with an equal block of scans with saturation off-resonance. The steady-state NOE,[36] η_{j-i}, for a proton i when proton j is saturated, is given by:

$$\eta_{j-i} = \sigma_{ij}/\rho_i = 0.1\gamma 4h^2 r_{ij}^{-6}\tau_c T_1 \qquad (1)$$

where σ_{ij} is the cross-relaxation rate, $\rho_i(T_1^{-1})$ the selective spin–lattice relaxation rate of proton i, r_{ij} is the interproton distance, and τ_c is the reorientation time of the i–j vector, estimated[29] as 3 ns for a 7 kDa protein. For rapidly relaxed protons, the selective ρ_i may be replaced by the nonselective ρ_i.[37] For the equation

$$Fd^{ox} + e^- \underset{k_{ox}}{\overset{k_{red}}{\rightleftarrows}} Fd^{red}$$

the intensity of signal i in Fd^{ox} with, I_i, and without, $I_i°$, saturating the corresponding signal in Fd^{red}, defines the saturation factor[38]

$$F_i = I_i/I_i° = \frac{\rho i}{\rho_i + k_{red}} \qquad (2)$$

The conventional n-type COSY spectrum[39] (MCOSY) was recorded in the magnitude mode, with 256 $t1$ values of 512 scans, each consisting of 1024 $t2$ points. The data were processed using 0°-shifted sine-squared window functions over 256 points in both dimensions and zero-filled to 1024 × 1024 data points. TOCSY[40] spectra were recorded at 400 MHz with rapid repetition pulsing conditions[40,41] (3.3 s^{-1}) to detect correlation from broad resonances (12.4-ms spin lock using WALTZ-16, with 256 $t1$ values of 640 scans, each with 1024 $t2$ points over a sweep width of 13.508 kHz). Additional TOCSY spectra, under slow repetition conditions (0.7 s^{-1}) to detect correlations for narrow signals (100-ms spin lock using MLEV-17, with 512 $t1$ blocks of 128 scans, each with 2048 $t2$ points over 10.0 kHz), were also collected. The data were apodized by 30°-shifted sine-squared function and zero-filled to 2048 × 2048 points prior to Fourier transformation. Base-line corrections in $f2$ were applied to the rapid repetition data. NOESY[42] data for the rapidly relaxed Cys signals were recorded at 500 MHz using a WEFT-NOESY pulse sequence,[43] with a pulse repetition rate of 7 s^{-1} and a delay of 65 ms after the initial 180° pulse prior to initiating the standard NOESY pulse sequence. The data consisted of 512 $t1$ blocks of 512 scans, each consisting of 1024 $t2$ points, and were apodized at 256 $t1$ × 256 $t2$ points by a 30°-shifted sine-bell-squared window function. The slow-repetition NOESY experiment was collected at 500 MHz with a 300 ms mixing time; the data matrix and processing are the same as for the TOCSY data. The EXSY[42] experiment to detect saturation transfer between Fd^{ox} and Fd^{red} was performed at 500 MHz on a 4.6 mM sample which was half-reduced, at 30 °C and 50 °C with a mixing time of 3 ms, a repetition rate of 0.7 s^{-1}, and 256 $t1$ blocks of 256 scans, each consisting of 2048 $t2$ points. The processing was the same as for the NOESY spectra. All 2D data processing was performed on a SUN Sparc station using the Biosym FELIX software.

Results

Oxidized Fd. The 500-MHz ^1H NMR spectrum of oxidized 4Fe *Tl* Fd (Fd^{ox}) in ^2H_2O, pH 7.5 at 30 °C, collected under nonsaturating conditions (repetition rate 0.4 s^{-1}), is illustrated in Figure 3A. Signals to the low field of 5.5 ppm belong to three classes of resonances: contact-shifted and strongly relaxed protons from the cysteines coordinated to the cluster irons (labeled *a–g, i*); the side-chain protons from the lone aromatic residue, Phe24 (labeled *j, k*); and slowly exchanging (and inefficiently relaxed) labile peptide protons (marked by asterisks). The high-field window exhibits two resolved resonances, *y, z*, each with three-proton intensity, indicative of methyl groups. The pattern of the weakly relaxed proton signals in the 1–5 ppm window is very similar to that previously reported[29] for the 3Fe *Tl* Fd^{ox}, indicating that the overall folding patterns for the two forms of the protein are homologous. The super-WEFT spectrum of the same sample, collected under conditions which leave the intensity of peaks with $T_1 \lesssim 10$ ms intact, partially suppresses the intensity of peaks with $T_1 \sim 30$ ms (*i.e.*, peaks *e, i*) and essentially completely suppresses resonances with $T_1 > 50$ ms, as shown in Figure 3B. This trace reveals several additional strongly relaxed signals, in particular those labeled *l, m, n*, which retain close to 100% intensity and hence relax with $T_1 \lesssim 10$ ms. The strongly relaxed resonance, *h*, is also observed clearly upon suppressing the nearby peptide NH signals. The upfield resolved resonance, *y*, is clearly a methyl peak, with $T_1 \sim 10$ ms. The chemical shift of the labeled signals are listed in Table 1; nonselective T_1 values for resolved signals are also included.

The temperature dependence of the chemical shifts for the resolved contact-shifted resonance, *a–g*, is plotted against

(36) Neuhaus, D.; Williamson, M. *The Nuclear Overhauser Effect in Structural and Conformational Analysis*; VCH Publications: New York, 1989.
(37) La Mar, G. N.; de Ropp, J. S. In *Biological Magnetic Resonance*; Berliner, L. J., Reuben, J., Eds.; Plenum Press: New York, 1993; Vol. 12, pp 1–78.
(38) Sandström, J. *Dynamic NMR Spectroscopy*; Academic Press: New York, 1982.
(39) Bax, A. *Two-Dimensional NMR in Liquids*; Reidel Publishing Co.: Dordrecht, The Netherlands, 1982.
(40) Bax, A.; Davis, D. G. *J. Magn. Reson.* **1985**, *65*, 355–360. Cavanagh, J.; Rance, M. *J. Magn. Reson.* **1990**, *88*, 72–85.
(41) Sadek, M.; Brownlee, R. T. C.; Scrofani, S. D. B.; Wedd, A. G. *J. Magn. Reson. Ser. B* **1993**, *101*, 309–314.
(42) Jeener, B. H.; Meier, P.; Bachmann, P.; Ernst, R. R. *J. Chem. Phys.* **1975**, *71*, 4546–4553.
(43) Chen, Z.; de Ropp, J. S.; Hernández, G.; La Mar, G. N. *J. Am. Chem. Soc.*, in press.

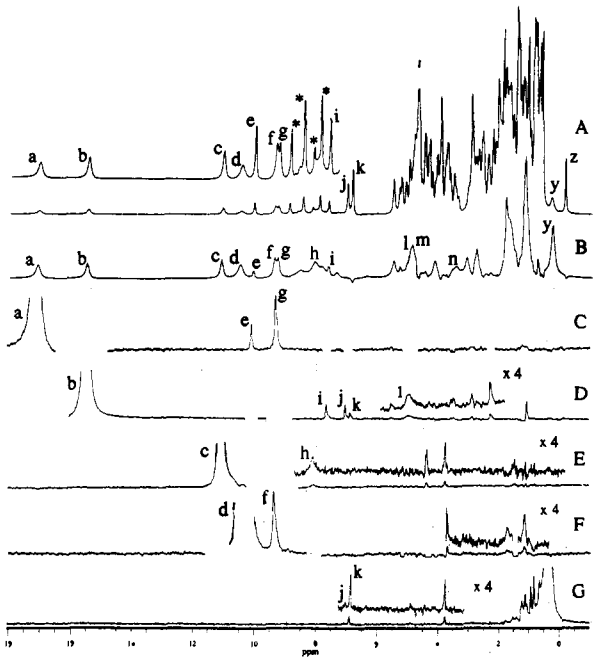

Figure 3. (A) 500-MHz ^{1}H NMR spectrum of 9.2 mM 4Fe *Tl* Fd^{ox} in ^2H_2O, pH 7.5, at 30 °C, collected under nonsaturating conditions (repetition rate 0.4 s^{-1}). Contact shifted Cys resonances are labeled *a–g*, the Phe 24 aromatic ring protons are labeled *j*, *k*, and two upfield methyls, one strongly relaxed and the other assigned to Val 23, are labeled *y*, *z*, respectively. Slowly exchanging peptide protons in the low-field window are marked by asterisks. (B) Super-WEFT trace of the same sample collected with a repetition rate of 20 s^{-1} and a delay time of 20 ms, which emphasizes very rapidly relaxed (T_1 < 10 ms) resonances in both the resolved (*a–i*, *z*) and unresolved (peaks *l*, *m*, *n*) spectral window. Note that peaks with T_1 > 50 ms are essentially completely suppressed. Traces C–G are steady-state NOE difference traces obtained upon saturating the resonances, *a*, *b*, *c*, *d*, and *y*, respectively, as shown with the vertical arrow. NOEs to other Cys protons are labeled as in A. The insets to D–G are vertical expansions by 4×.

reciprocal absolute temperature (Curie plot) in Figure 4A. All resonances exhibit anti-Curie behavior, as expected for the diamagnetic (S = 0) ground state.[2,3,28] The chemical shift of 0.85 ppm for the upfield relaxed methyl peak, *y*, is temperature independent, indicating that it experiences strong relaxation but no contact shift.

Reduced Fd. The 500-MHz ^{1}H NMR spectrum of a ~1:1 mixture of reduced 4Fe *Tl* Fd (Fd^{4ed}) and Fd^{ox} in ^2H_2O, pH 7.5 at 30 °C, is illustrated in Figure 5A; the resolved Fd^{ox} peaks are labeled as in Figure 3A. The new resonances, which are uniquely attributed to Fd^{red}, are labeled *a′–i′*, *l′*, *n′*. The peaks in Figure 5A are slightly broader for both Fd^{ox} and Fd^{red} compared to those observed when only one or the other is present, due to exchange effects in the slow exchange regime[38] (see below). The line widths and T_1 values for those resonances, recorded for a completely reduced sample, are listed in Table 1. Fd^{red} generally exhibits larger contact shifts and broader lines[11,16,22,23] with shorter T_1 values than Fd^{ox}, which is consistent with a paramagnetic (S = $^1/_2$) ground state[2,3,28] for the former. The influence of temperature on the chemical shifts for 4Fe *Tl* Fd^{red} is illustrated in the Curie plot in Figure 4B. Five of the resolved low-field resonances, *b′*, *d′*, *f′*, *l′*, *i′*, exhibit Curie-like behavior (contact shift decreases with increasing temperature), while the other five low-field peaks, *a′*, *c′*, *g′*, *e′*, *h′*, display anti-Curie behavior (contact shift increases with increasing temperature).

2D NMR of Oxidized Fd. The location of the coordinated Cys resonances was initiated for 4Fe *Tl* Fd^{ox} because of its narrower and less strongly relaxed resonances (Table 1). Magnitude COSY, MCOSY, spectra identified one two-spin (*d*, *f*) and two three-spin (*a*, *g*, *e* and *c*, *h*, *m*) systems involving the hyperfine shifted and relaxed resonances as candidates for the four Cys (not shown; see supplementary material). The upfield broad methyl peak *y* failed to exhibit a MCOSY cross peak. The TOCSY spectrum with an appropriately short spin-lock time,[37,41] illustrated in Figure 6, reveals the same two three-spin systems as MCOSY, expands one MCOSY-detected two-spin system to a three-spin system (*d*, *f*, *n*), identifies a new two-spin system (*b*, *ℓ*), and exhibits a clear cross peak (labeled 8) between the upfield relaxed methyl peak *y*, and a resonance at 2.80 ppm. The only hyperfine/relaxed peak for which scalar connectivity could not be detected is peak *i*.

The 30 °C WEFT-NOESY spectrum collected under rapid pulsing conditions to enhance the sensitivity, with a mixing time of 5 ms optimized for the rapidly relaxed signals,[37] exhibited detectable intra-Cys cross peaks of variable intensity for the sets of resonances (*a*, *g*), (*b*, *ℓ*), and (*c*, *h*) (not shown; see supplementary material). A steady-state NOE from peak *b* to peak *i* (Figure 3D) identifies peak *i* as part of the three-spin system (*b*, *ℓ*, *i*). Hence the combination of TOCSY, NOESY, and steady-state NOEs locates four three-spin systems accounting for all hyperfine shifted resonances expected from the four Cys coordinated to the cluster. The relative intensities of the pairs of cross peaks in each Cys spin system, however, do not provide an unambiguous differentiation of Cys C_βH and C_αH signals in any of the 2D experiments.

The TOCSY spectrum with a 100-ms mixing time (not shown) confirms the peptide NH origin for the slowly relaxing resonances in the 6–8 ppm region of Figure 3A by detecting the diagnostic cross peak to C_αHs (marked with asterisks in Figure 6B). Moreover, the cross peak between nonlabile resonances *j*, *k*, with relative intensity 2:3, identifies them as the Phe 24 ring protons. In the 300-ms mixing time NOESY, a cross peak between the upfield methyl peak *z* and the Phe 24 ring proton (not shown) identifies Val 23 $C_\gamma H_3$ and confirms a folding topology similar to those in 3Fe *Tl* Fd^{ox} in solution[29] and *Dg* 3Fe Fd^{ox} in single crystal.[33]

Steady-State NOEs in Oxidized Fd. In order to place the assignment of individual Cys protons on a more quantitative basis, as well as to provide information on spatial contacts between the Cys and the diamagnetic polypeptide backbone, each of the resolved contact shifted and/or relaxed resonances was saturated by a selective decoupler pulse of 105 ms. The relevant resulting steady-state NOE difference spectra are illustrated in Figures 3C–G. Thus, saturating peak *a* in Figure 3C results in steady-state NOEs to peaks *e* and *g* which, with the T_1 values in Table 1, yields[36,37] $\sigma_{ag} \sim 5\ s^{-1}$ and $\sigma_{ae} \sim -1\ s^{-1}$ via eq 1. Those, in turn, translate to $r_{ag} \sim 1.6$ and $r_{ar} \sim 2.3$ Å via eq 2, dictating that *a*, *g* are geminal C_βHs and *e* is the C_αH for Cys A. While the T_1 for peak *ℓ* is not directly determined, the steady NOE to peak *i* upon saturating peak *b* in Figure 3D, together with the T_1 for *i* in Table 1, yield $\sigma_{bi} \sim 1\ s^{-1}$ and $r_{bi} \sim 2.3$ Å; hence *b*, *ℓ* are C_βHs and *i* is the C_αH for Cys B. Saturating peak *c* (Figure 3E) or *d* (Figure 3F) results in only one NOE to a hyperfine shifted peak in each case (*h*, *f*, respectively); the T_1 values for these resolved peaks indicate $\sigma \sim -5\ s^{-1}$ in each case, identifying *c*, *h* and *d*, *f* as C_βH geminal partners for Cys C and Cys D, respectively. The intensities of the resonances in the super-WEFT trace in Figure 3B indicate that the two C_αH peaks, *m* and *n*, for Cys C and D, are as rapidly relaxed as either of the C_βHs of the same residue. In contrast, the C_αHs for Cys A and B exhibit T_1 values significantly longer than either of their C_βHs (Table 1).

The saturation of the upfield relaxed methyl resonance, *y*, illustrated in Figure 3G, exhibits NOEs to Phe 24 ring protons *j*, *k* as well as to a peak at 3.76 ppm.

Cys Assignments in Reduced Fd by Magnetization Transfer. Facile electron exchange between 4Fe *Tl* Fd^{ox} and Fd^{red} allows the transfer[15,16,37,38] of the complete assignments for Fd^{ox} to Fd^{red}. The spectrum of a ~1:1 mixture of Fd^{ox} and Fd^{red} is shown in

Table 1. ^{1}H NMR Spectral Parameters for the Assigned Cluster Ligated Cys in *Thermococcus litoralis* 4Fe Ferredoxin[a]

				Fd^{ox}						Fd^{red}						
Cys	cys[b] assignment	peak label[c]	peak assignment[d]	δ_{obs}[e]	line width[f]	T_1[h]	δ_{con}[i]	$\bar{\delta}_{con}(C_\beta H)$[k]	$\frac{\delta_{con}(C_\beta H)}{\delta_{con}(C_\beta H')}$	δ_{obs}[e]	line width[f]	T_1[h]	δ_{con}[i]	$\bar{\delta}_{con}(C_\beta H)$[k]	$\frac{\delta_{con}(C_\beta H)}{\delta_{con}(C_\beta H')}$	VT[l] slope
A	13 (II)	a	$C_\beta H'$	17.07	70	7.5	14.1	10.2	0.45	46.9	200	7.2	43.9	36.8	0.68	AC
		g	$C_\beta H$	9.30	~50	14.1	6.3			32.7	130	13.7	29.7			
		e	$C_\alpha H$	10.08	17	30.4	5.6			18.9	~70	26	14.4			
B	16 (III)	b	$C_\beta H$	15.49	49	11.0	12.5	7.3	6.3	35.3	160	12.1	32.3	21.4	3.1	C
		l	$C_\beta H'$	5.0	~120[g]	~2[j]	2.0			13.5	~240	~3	10.5			
		i	$C_\alpha H$	7.66	20	28	3.2			13.05	~75	16.7	8.6			
C	51 (IV)	c	$C_\beta H$	11.10	41	12.3	8.1	6.6	1.6	34.1	165	4.9	31.1	23.3	2.0	AC
		h	$C_\beta H'$	8.1	~130	5.1	5.1			18.5	~250	5.4	155			
		m	$C_\alpha H$	4.9	>50[g]	<10[j]	0.4			7.0			2.4			
D	10 (I)	d	$C_\beta H'$	10.50	71	6.1	7.5	7.0	0.85	37.5	245	4.3	34.0	42.3	1.4	C
		f	$C_\beta H$	9.40	50	14.3	6.4			53.0	195	9.3	50.0			
		n	$C_\alpha H$	3.5	>50[g]	<10[j]	−1.0			−2.7	250	~4	−7.2			

[a] In ^2H_2O, pH 7.5 at 30 °C. [b] As assigned in text based on sequence in Figure 2. [c] As labeled in Figures 3–6. [d] $C_\beta H$, $C_\beta H'$ are the Cys β-methylene protons further from and closer to the iron, respectively. [e] Chemical shift, in ppm from DSS. [f] In Hz at 500 MHz, uncertainties ±10%. [g] Line width estimated in WEFT time (Figure 3B) or in steady-state NOE difference trace (Figure 3C–F). [h] In ms; uncertainties ±10%. [i] Estimated from null point or from intensity in Super-WEFT trace in Figure 3B. [j] Contact shift corrected for diamagnetic shift of 3.0 ($C_\beta Hs$) and 4.5 ppm ($C_\alpha H$). [k] $\bar{\delta}_{con}(C_\beta H)' = {}^1/_2(\delta_{con}(C_\beta H) + \delta_{con}(C_\beta H')$. [l] C (Curie) and AC (anti-Curie) temperature dependence in Figure 4.

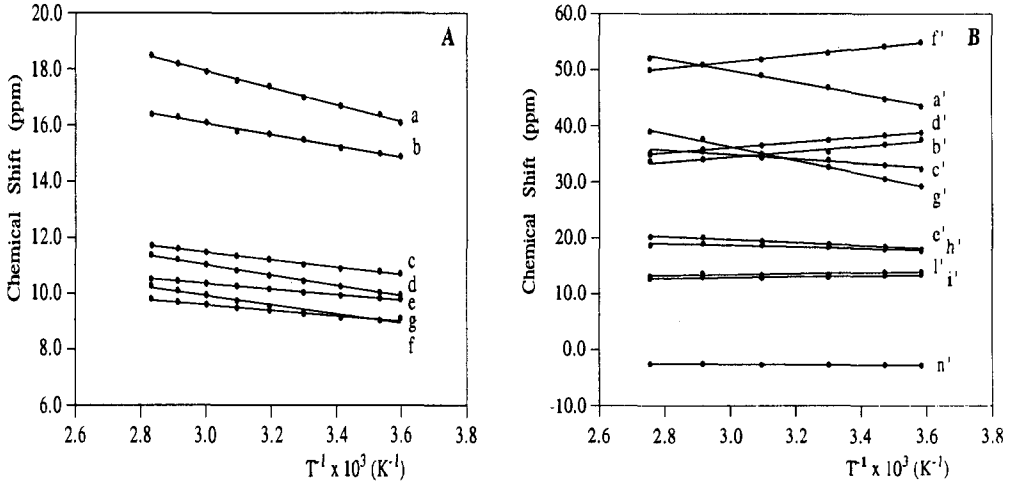

Figure 4. Plot of observed chemical shifts relative to DSS versus reciprocal absolute temperature (Curie plot) for the assigned resolved contact shifted Cys resonances from (A) oxidized 4Fe *Tl* Fd and (B) reduced 4Fe *Tl* Fd. The peaks are labeled as in Figures 3A and 5A.

Figure 5A, where the resonances for oxidized protons are labeled *a*,*b*, and those for the reduced are protein *a'*–*l'*. The 30 °C 2D EXSY spectrum of this sample, using a mixing time of 3 ms (shown in Figure 5C), exhibits nine intense cross peaks that pairwise connect the similarly labeled primed and unprimed peaks, cross-correlating the assignments between the two oxidation states. Two resonances, *l*, *m*, have their cross peaks too close to the diagonal to be detected at this temperature but yield the expected cross peak at 50 °C (not shown). The diamagnetic window exhibits too many artifacts to allow detection of a cross peak to the unresolved peak *n* for 4Fe *Tl* Fd^{ox}. However, direct saturation of the upfield peak *n'* of Fd^{red} exhibits saturation transfer to *n* (Figure 5B), providing the last correlation necessary to complete the assignment of the four Cys in each of the two oxidation states.

Sequence-Specific Cys Assignments. The $C_\beta H$ of Cys B (peak *b*) exhibits NOEs to both Phe 24 ring signals (Figure 3D), clearly identifying it as Cys 16 (III). Only Cys III is close enough to the Phe ring in the *Dg*[33] or *Bacillus thermoproteolyticus*[44] (*Bt*) Fd crystal structures (see Figure 1) to exhibit the observed NOEs. This has also been shown to be the case for the 3Fe Fd^{ox} from *Tl*,[29] *Dg*,[22] as well as from another hyperthermophile, *Pyrococcus furiosus* (*Pf*).[29] The Cys A signal *a* (as well as signal *g*, not shown) does not exhibit NOEs that aid in its assignment (Figure 3C). Signal *c* from Cys C exhibits NOEs (Figure 3E) primarily to 3.8 and 4.4 ppm, where the preliminary 2D data indicate 6–8 as yet unassigned resonances (not shown). The steady-state NOE from peak *f* of Cys D reflects the most informative pattern in the diamagnetic window, in particular a peak at ~3.0 ppm, where the 2D map indicates only Lys $C_\epsilon Hs$ resonate (not shown). The steady-state NOE is reproduced in Figure 7A next to the section of the TOCSY spectrum (100 ms mixing time) that maps out the spin system for a Lys[45] (cross peaks labeled 9(ε), 10(β), 11(δ), 12(γ)). It is observed that these four peaks in the 1D NOE correlate with the Lys TOCSY cross peaks 9–12, dictating that Cys D is in close proximity to this Lys side chain.

The peptide section of the NOESY spectrum (300 ms mixing time) reveals two cross peaks from this Lys peptide NH to an $C_\alpha H$ (labeled 13, Figure 7C) and to another peptide NH (labeled 14, Figure 7D), which the NOESY in Figure 7C (cross peaks 15, 16) and the TOCSY (data not shown) spectra show to arise from a Gly. The $C_\alpha H$–NH and the NH–NH NOESY cross peaks indicate[45] that the Lys and Gly are adjacent in the sequence and identifiy the candidates as Gly 30–Lys 31 (Figure 2). These two residues are present in the sequence of *Dg* Fd[32] and are placed in the crystal structure[33] of that protein in a highly conserved hydrophobic core such that Lys interacts solely with Cys 8 (I). Based on the strong sequence homology and apparent conservation of much of the folding topology, as revealed in a comparison NMR study of the 3Fe Fds,[29] we conclude that Cys D arises from Cys 10 (I) in 4Fe *Tl* Fd^{ox}. Definitive assignments to the resonance

(44) Fukuyama, K.; Nagahara, Y.; Tsukihara, T.; Katsube, Y.; Hase, T.; Matsubara, H. *J. Mol. Biol.* **1988**, *199*, 183–193.

(45) Wüthrich, K. *NMR of Proteins and Nucleic Acids*; John Wiley & Sons: New York, 1986.

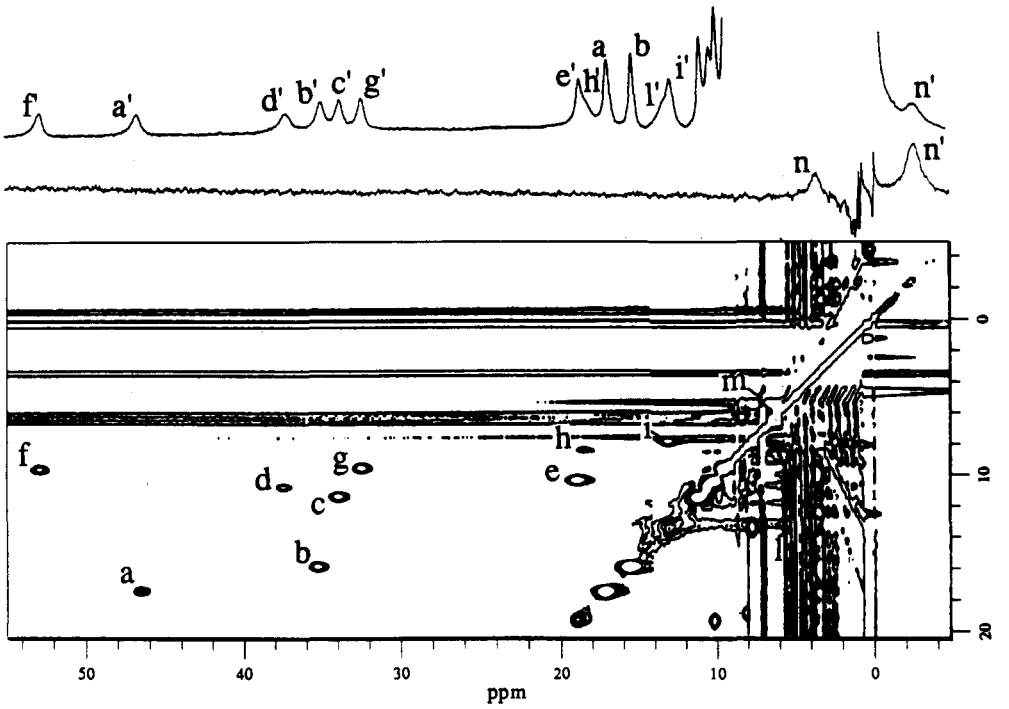

Figure 5. (A) 500-MHz ^1H NMR reference trace of a ~1:1 mixture of oxidized and reduced 4Fe *Tl* Fd in ^2H_2O, pH 7.5, at 30 °C. The resonances for Fd^{ox} are labeled *a–m*, as shown in Figure 3A, while those for the Fd^{red} are labeled *a–m'*, with the same label reserved for cross-correlated resonances. (B) 1D difference trace upon saturating the upfield resolved peak *n'* for Fd^{red}; note significant saturation transfer to peak *n* of Fd^{ox}. (C) Portion of the 3 ms mixing time NOESY (EXSY) spectrum illustrating the cross correlation of resonances between 4Fe *Tl* Fd^{ox} and Fd^{red}; the intense cross peaks are labeled with the letter for the correlated peak (unprimed in Fd^{ox}, primed in Fd^{red}).

in the diamagnetic window to discriminate between Cys A and Cys C are unsuccessful at this time.

The upfield methyl signal, *y*, exhibits a strong NOE to the Phe 24 ring signal *k* (Figure 3G). The short T_1 ~ 10 ms of *y*, when compared to that of Cys C_βHs, dictates that it is ≲5 Å from the iron.[29] The *Dg* Fd crystal structure[33] and sequence homology[32] to *Tl* Fd limits to four the number of residues with methyl groups within 5 Å of the cluster iron atoms. However, only one residue, Ile 55 in *Dg* Fd, is close to the Phe. Since this Ile, as well as a large portion of the sequence between Cys VI and Cys IV (Figure 2) is conserved in *Tl* relative to *Dg* Fd (Figure 1), we assign peak *y* to the $C_\delta H_3$ of Ile 56 in *Tl* Fd. The observed TOCSY cross peak identifies one of the C_γHs of the same residue.

Electron Self-Exchange. The rate of electron exchange is most readily measured by steady-state saturation-transfer techniques.[38] Saturating the 4Fe *Tl* Fd^{red} peak *a'* in a 1:1 mixture of Fd^{ox}:Fd^{red} leads to a ~0.6 saturation factor for Fd^{ox} peak *a*, which with the T_1 = 7.5 ms for peak *a* yields k_{red} ~ 1 × 10^2 s^{-1}. The ~1:1 composition of the mixture of Fd^{ox}, Fd^{red} in the 4.6 mM protein solution yields an electron self-exchange constant ~5 × 10^4 M^{-1} s^{-1} at 30 °C. The facile electron exchange rate and the presence of only two oxidation states of *Tl* Fd in the ^1H NMR spectra indicate that only the iron–sulfur cluster is redox active.

Discussion

Identification of Hyperfine Shifted/Relaxed Resonances. The combination of the 2D experiments and steady-state NOEs identified all 12 hyperfine shifted proton signals from the four ligated Cys in the oxidized 4Fe *Tl* Fd. The most effective 2D experiment was found to be TOCSY, as had been previously demonstrated for the oxidized 2 × 4Fe *Cp* Fd. However, while the 2D experiments are unable to clearly distinguish between α- and β-protons within a single Cys due to the variable T_1 values and line widths of the resonances, these distinctions could be effected by steady-state NOEs. The transfer of the assignment for all 12 resonances from the oxidized to the reduced *Tl* Fd via magnetization transfer provides the first example in which all resonances for the ligated Cys have been identified in both oxidation states of an iron–sulfur cluster protein. The fact that the short mixing time TOCSY spectrum revealed a scalar cross peak to the strongly relaxed $C_\delta H_3$ of Ile 56 provides encouraging evidence that scalar correlation should be able to contribute significantly to mapping out the relaxed but noncoordinated residues near the cluster. The identification of such residues is crucial to the ^1H NMR solution structure determination of Fd.[46] Such studies, however, require much more extensive data and are well outside the scope of this study.

Sequence-Specific Assignments of Cys. Two of the Cys (Cys B and Cys D) are assigned on the basis of identifying, by standard 2D NMR methods,[45] the spin systems for the "diamagnetic" residues that exhibit NOEs when the relevant Cys $C_\beta H$ signals are saturated. Even these assignments require the assumption that the molecular topology of 4Fe *Tl* Fd is very similar to that of the reference protein, *Dg* Fd.[33] This assumption appears reasonable near the iron cluster.[29] The cluster environment and the hydrophobic core appear remarkably conserved in all structurally characterized bacterial Fds, including 2 × 4Fe *Peptococcus aerogenes* (*Pa*) Fd,[47] 3Fe *Dg* Fd,[33] 4Fe *Bt* Fd,[44] and both the 3Fe and 4Fe clusters of the 7Fe Fd for *Azotobacter vinelandii*,[48] *Av*.

Assuming the folding topology of *Tl* Fd is similar to that of *Dg* Fd, the present assignment of Cys B to Cys 16 (III) is definitive because the identity of signals *j*, *k* for the ring of Phe 24 is unambiguous.[29] The assignment of Cys D to Cys 10 (I) on the basis of the NOEs to three of the signals of Lys 31, however, will be definitively confirmed only upon assigning all signals for the protein. The danger in simplistic assignments of Cys based on NOEs to the aliphatic portion of the diamagnetic envelope is

(46) Teng, Q.; Zhou, Z. H.; Smith, E. T.; Busse, S. C.; Howard, J. B.; Adams, M. W. W.; La Mar, G. N. *Biochemistry*, in press.
(47) Adman, E. T.; Sieker, L. C.; Jensen, L. H. *J. Biol. Chem.* **1976**, *251*, 3801–3806. Backes, G.; Mino, Y.; Loehr, T. M.; Meyer, T. E.; Cusanovich, M. A.; Sweeney, W. V.; Adman, E. T.; Sanders-Loehr, J. *J. Am. Chem. Soc.* **1991**, *113*, 2055–2064.
(48) Stout, C. D. *J. Mol. Biol.* **1989**, *205*, 545–555.

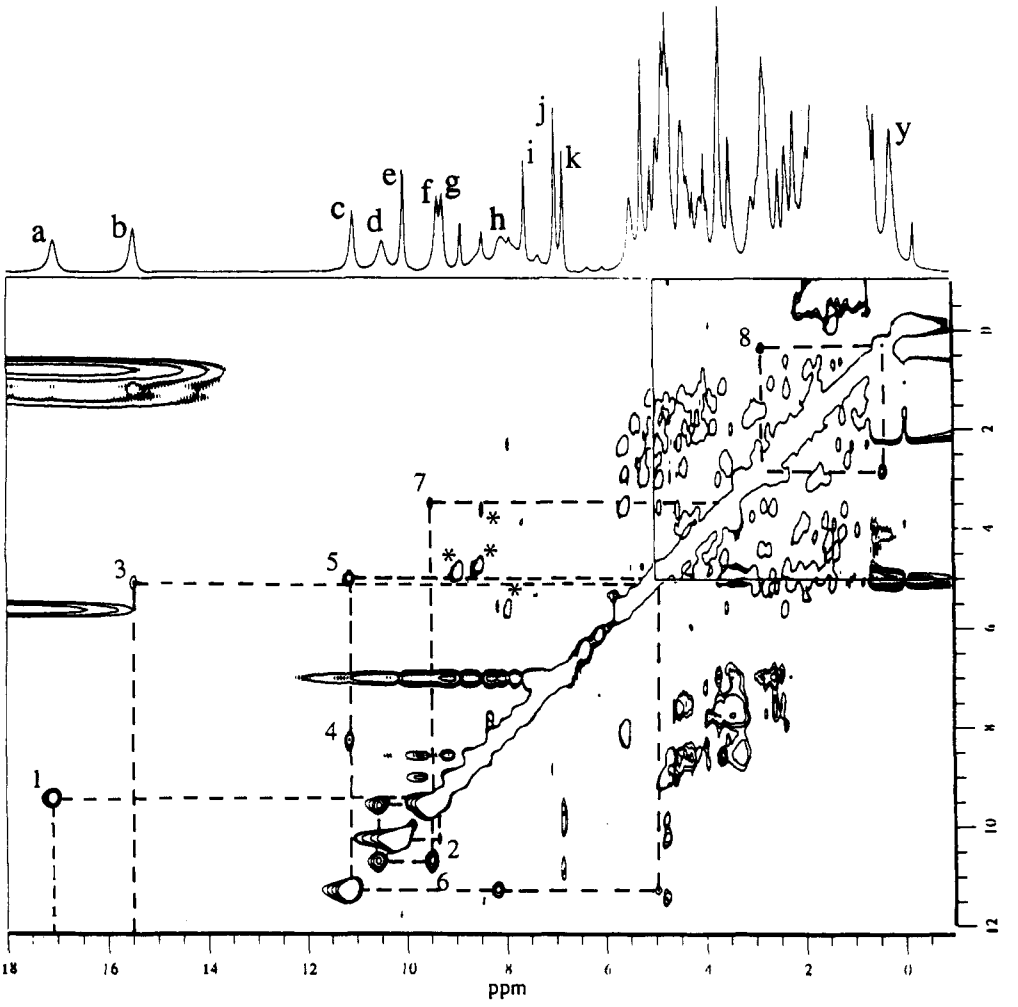

Figure 6. (A) Reference trace for 4Fe *Tl* Fd^{ox} in ^2H_2O, pH 7.5, at 30 °C, collected at a repetition rate of 4.4 s^{-1} to emphasize relaxed resonances; the peaks are labeled as in Figure 3A. (B) 12.4 ms mixing time TOCSY spectrum illustrating the two cross peaks that correlate the scalar connectivities for the four three-spin systems for the ligated cysteines. Cross peaks 1, 2 correlate *a*, *g*, and *e*; cross peak 3 correlates *b* and *l*; cross peaks 4, 5 correlate *c*, *h*, and *m*; and cross peaks 6, 7 correlate *d*, *f*, and *n*. The scalar connection between the strongly relaxed methyl peak *y* and a proton at 2.80 ppm is labeled 8.

dramatically illustrated in the steady-state NOE difference traces in Figure 3. Thus, saturation of peaks *c*, *d*, and *y* results in each exhibiting a relatively strong NOE to a peak at 3.76 ppm (Figures 3E,F,G, respectively), suggesting that protons *c*, *d*, and *y* are near a common residue, and hence the starting point of a sequence-specific assignment. Cursory examination of a 100 ms mixing time TOCSY map at 30 °C, however, revealed at least six distinct protons with chemical shifts within the uncertainty of 3.76 ppm (not shown). When the experiments depicted in Figures 3E–G were repeated at 60 °C (not shown), it was observed that the three signals at 3.76 ppm, which exhibit NOEs in Figures 3E,F,G, result from at least three different protons. Once again, the identification of these signals will require the complete sequence-specific assignment for the protein. Such studies are in progress.

The assignment of the remaining two Cys A, C, however, can still be effected by detailed consideration of the geometric properties of cluster-coordinated Cys in a variety of Fds, the relaxation properties of the individual protons of a given Cys,[49] and the earlier ^1H NMR data[29] on the 3Fe *Tl* Fd^{ox}. Examination of the available X-ray crystal structures for cubane Fd, 8Fe *Pa* Fd,[47] 4Fe *Bt* Fd,[44] 3Fe *Dg* Fd,[33] and 7Fe *Av* Fd[48] reveals a conserved pattern for the geometry of the four ligating Cys I–IV in each of these proteins.[50] Two of the ligating Cys, I and IV, invariably have $C_\alpha H$ oriented toward the cluster and only <3.5 Å from a cluster iron, which is comparable to the cluster proximity of one $C_\beta H$ (labeled $C_\beta H'$ in Table 1) and ~1.5 Å closer than the other $C_\beta H$ (labeled $C_\beta H$ in Table 1). The two $C_\beta Hs$ are readily recognized by their expected differential relaxation properties[49] (see Table 1). Hence, Cys I and IV possess $C_\alpha Hs$ whose T_1 values should be necessarily shorter than that for at least one, and likely both, $C_\beta H$ of the same residue. In contrast, Cys II and III invariably have $C_\alpha Hs$ oriented away from the cluster with distances to the nearest cluster iron of ~5.0 ± 0.2 Å, *i.e.*, significantly further from the iron than one or both $C_\beta H$ of the same residue. In both crystallographically characterized 3Fe clusters,[33,48] it is the iron that would ligate to Cys II that is deleted. In 3Fe *Pf* Fd, position II in the consensus sequence is occupied by Asp 14,[28] and the same iron that would ligate Cys II has been proposed to be deleted in 3Fe *Tl* Fd.[28,29]

The previous identification[29] of the hyperfine shifted Cys signals in 3Fe *Tl* and *Pf* Fd^{ox} located one Cys whose $C_\alpha H$ exhibits a large contact shift and a relatively long T_1 indicative of a distance to the iron that is greater than that for $C_\beta Hs$, and two residues with $C_\alpha H$ with smaller contact shifts that are relaxed comparable to

(49) Busse, S. C.; La Mar, G. N.; Howard, J. B. *J. Biol. Chem.* **1991**, *226*, 23714–23723.

(50) In the 2 × 4Fe *Pa* Fd[45] and 4Fe:3Fe *Av* Fd[46], Cys I–IV are defined the same as for *Dg* and *Tl* Fd in Figure 2. Cys I–IV for the second clusters are those reflected by the pseudo-2-fold symmetry[48] of the *Pa* Fd, i.e., Cys 8, 11, 14, and 46 for the cluster homologous to *Dg* and *Tl* Fd, and Cys 36, 39, 42, and 18, respectively, for the second cluster.

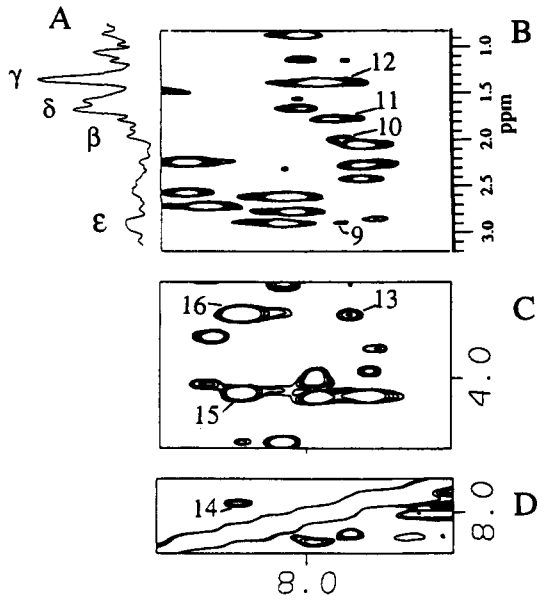

Figure 7. Correlation between steady-state NOE detected upon saturating Cys D peak *f* (A) with the resonance of a Lys observed in a portion of the 100 ms TOCSY spectrum (B), with cross peaks from $C_\varepsilon H$, $C_\beta H$, $C_\delta H$, and $C_\gamma H$ labeled 9–12, respectively. Portions of the 300 ms NOESY spectrum with the Lys NH cross peaks to the $C_\alpha H$ and NH of the adjacent residue (cross peaks 13, 14) are shown in (C, D). The NOESY map in C also reveals that the residue adjacent to the Lys is a Gly ($C_\alpha H$ cross peaks 15, 16).

a $C_\beta H$, consistent with the fact that Cys 13 (II) is not ligated in the 3Fe cluster. Moreover, the one sequence-specifically assigned[29] Cys 16 (III) of 3Fe *Tl* Fd^{ox} (and Cys 17 (III) of 3Fe *Pf* Fd^{ox}) exhibits the weakly relaxed $C_\alpha H$ precisely as predicted by the cluster geometry[33] described above. The four located Cys for the present 4Fe *Tl* Fd^{ox} exhibit relaxation properties which show that two Cys, A and B, have $C_\alpha Hs$ relaxed much more weakly than $C_\beta Hs$ and hence musdt originate from Cys II and Cys III. The NOE to Phe 24 assigns Cys B to Cys 16 (III), confirming the correlation. Therefore, Cys A, with the weakly relaxed $C_\alpha H$ in 4Fe *Tl* Fd, can be directly assigned to Cys 13 (II), which was not ligated in 3Fe Fd.[28,29] This leaves only Cys C, which must arise from the remaining Cys 51 (IV) in 4Fe *Tl* Fd.

The above analysis suggests that the identification and characterization of relaxation properties of $C_\alpha Hs$ for coordinated Cys in Fds likely provides valuable information for sequence-specifically assigning the ligating Cys. The assignment[23] of the weakly relaxed resolved $C_\alpha H$ signals to Cys (II)[11,40] in 2 × 4Fe oxidized *Cp* and *Cau* Fd is consistent with expectations. Since Cys III is always close to the conserved aromatic residue[25,28] (see Figure 1) in single cluster Fds, it should be straightforward to assign two of the four ligating Cys in a 4Fe Fd, provided the $C_\alpha H$ resonance is sufficiently resolved to allow estimates of its T_1. In a 3Fe cluster protein, the assignment from the NOE to the conserved aromatic residue and the $C_\alpha H$ relaxation properties[29] are redundant but provide important checks on the validity of the approach.

Cluster Electronic/Magnetic Properties. The Curie plots in Figure 4B reveal that the $C_\beta Hs$ for two Cys, B, D assigned to Cys10(I) and Cys16(III) of 4Fe *Tl* Fd^{red}, respectively, exhibit Curie-like behavior, while the two Cys A,C assigned to Cys13-(II) and 51(IV) respectively, display anti-Curie behavior. Based on the reasonable assumption[9,14,16,22] that the intermediate spin states for the two iron pair are $S_A = 9/2$ and $S_B = 4$,[51,52] this dictates that the valence-delocalized pair of iron atoms in 4Fe *Tl* Fd^{red} is ligated to Cys 10 (I) and Cys 16 (III). The sequence-specific assignments of the ligated Cys in reduced 2 × 4Fe Fd from both *Cp* and *Cau* have shown[23] that the resonances which exhibit Curie rather than anti-Curie temperature dependence, and hence arise from the valence-delocalized $2Fe^{2.5+}$ ligated Cys, also arise from the homologous Cys 8,37 (I) and Cys 14,43 (III) in both clusters.[50]

We and others had previously shown[29,30] that the temperature dependences of the hyperfine shifts of 3Fe Fd^{ox} exhibit deviations from Curie law that reflect a characteristic 2:1 asymmetry in the spin coupling hierarchy, with one Cys exhibiting Curie-like behavior and the other two displaying anti-Curie behavior. The pattern of Cys contact shifts for the $C_\beta Hs$, the unique low-field hyperfine shift for only one $C_\alpha H$, and the similar 1D NOE pattern[29] indicate that the Cys with anti-Curie temperature dependence in 3Fe *Tl* Fd^{ox} that pairs with the assigned Cys 16 (III) is analogous to Cys D of the 4Fe *Tl* Fd described here. Hence the 2:1 asymmetry in 3Fe *Tl* Fd appears to pair Cys 10 (I) and Cys 16 (III). A similar conclusion has been reached for the 3Fe Fd^{ox} from *Dg*.[22] It thus appears as if the structural basis for the magnetic/electronic asymmetry is conserved between *Cp*, *Cau* 2 × Fe Fd^{red}, and *Tl* 4Fe Fd^{red}, between the 3Fe Fd^{ox} and 4Fe Fd^{red} clusters of *Tl*, and between the 3Fe Fd^{ox} of *Tl*[29] and *Dg*.[22] The generality of this pairing of iron atoms, as well as the exact structural basis in any one Fd, remains to be determined since the crystal structures are available for only one of these Fd, oxidized 3Fe *Dg* Fd.[33]

Cys Contact Shift Patterns. The pattern of the dominant contact shifts for coordinated Cys can provide, in principle, information on the orientation of the Cys relative to the cluster, as well as the magnetic environment.[11,49,52] To date, primarily $C_\beta H$ contact shifts have been considered, likely because insufficient assignments on $C_\alpha Hs$ were available. The simple angular dependence in terms of the Fe–S–C_β–H_β dihedral angle[11,15,29,30] is complicated by extensive spin delocalization into the sulfur lone pairs,[52] each of which can similarly interact with a $C_\beta H$. The contact shifts, δ_{con}, referenced to the diamagnetic Cys position, as well as the ratio of the contact shifts for $C_\beta H/C_\beta H'$ and the mean shifts for $C_\beta H$, $C_\beta H'$, $\delta_{con}(C_\beta H, C_\beta H')$ for 4Fe *Tl* Fd^{ox} and Fd^{red}, are included in Table 1. It is noted that the patterns of $C_\beta H$ shifts are similar in the alternate redox states, consistent with similar but not necessarily identical cluster environments in the alternate cluster oxidation states.

Perhaps more interesting is an apparent correlation of the magnitude of the $C_\alpha H$ contact shift with its orientation with respect to the cluster. It is noted that the Cys with the more weakly relaxed $C_\alpha Hs$ (Cys 13 (II) and Cys 16 (III)) also exhibit much larger contact shifts than the Cys with more strongly relaxed $C_\alpha Hs$ (Cys 10 (I) and Cys 51 (IV)). Spin delocalization in the S–C_β–C_α–H fragment, as observed for *J* spin coupling in diamagnetic systems[54] and for spin delocalization in Ni(II) amine complexes,[55] should follow approximately a $\cos^2\phi$ dependence of the dihedral angle, ϕ, in this case the S–C_β–C_α–H_α angle; spin density in sulfur lone pairs should not interfere as seriously as for Fe–S–C_β–H coupling.[52] The Fd crystal structure data[33,44,47,48] reveal that the Cys with $C_\alpha Hs$ more remote from the cluster (II, III) have S–C_β–C_α–H angles 155–180° ($\cos^2\phi = 0.9 \pm 0.1$), while the two Cys with $C_\alpha Hs$ nearer the iron (I and IV) have S–C_β–C_α–H angles near 60° ($\cos^2\phi = 0.25 \pm .08$). Hence the magnitude of the Cys $C_\alpha H$ shift may provide direct information

(51) It is noted that recent studies on model cubane iron–sulfur model compounds[52] indicate that the intermediate spins are $^7/_2$, 3 instead of $^9/_2$, 4. However, in either case the valence-delocalized pair possesses the larger intermediate spin, so that the differentiation of the pairs of Cys on the basis of Curie and anti-Curie temperature dependence is unaffected.

(52) Mouesca, J.-M.; Rius, G.; Lamotte, B. *J. Am. Chem. Soc.* **1993**, *115*, 4714–4731.
(53) Carter, C. W.; Kraut, J.; Freer, S. T.; Xuong, N.-H.; Alden, R. A.; Bartsch, R. G. *J. Biol. Chem.* **1974**, *249*, 4212–4225.
(54) Karplus, M. *J. Am. Chem. Soc.* **1963**, *85*, 2870–2871.
(55) Ho, F. F.-L.; Reilley, C. N. *Anal. Chem.* **1969**, *41*, 1835–1841.

on the orientation of the ligating Cys. The qualitative correlation between the crystallographically predicted orientation of a ligated Cys $C_\alpha H$ and its relaxation and contact shift pattern is qualitatively consistent with reported assignments for *Dg* 3Fe and 4Fe Fd,[22,30] *Cp* and *Cau* 2 × 4Fe Fd,[23] and HiPiP.[19-21,56] The general utility of $C_\alpha H$ contact shifts and relaxation properties as probes for Cys orientation is being explored in a variety of Fds.

Acknowledgment, One of us, A.D., wants to thank the University of Valencia for a grant of the "Programa de Formación del Profesorado del Ministerio de Educación y Ciencia (Spain)". This research was supported by grants from the National Science Foundation, DMB 91-04018 (G.N.L.), DMB 91-05150 (M.W.W.A.), and the National Institutes of Health, GM 45597 (M.W.W.A.).

(56) The four Cys in HiPiP[53] do not exhibit the pairwise differentiation in $C_\alpha H$ orientations. However, the residue with a large S–C_β–$C_\alpha H$ angle (Cys 77) also exhibits the largest $C_\alpha H$ contact shift.[14,18,19]

Supplementary Material Available: Figures showing MCOSY and NOESY spectra from Cys resonances (2 pages). This material is contained in many libraries on microfiche, immediately follows this article in the microfilm version of the journal, and can be ordered from the ACS; see any current masthead page for ordering information.